J Biol Inorg Chem (2013) 18:277–286
DOI 10.1007/s00775-012-0972-2

ORIGINAL PAPER

Interactions of disulfide-constrained cyclic tetrapeptides with Cu^{2+}

Liyun Zhang · Zhaofeng Luo · Lidong Zhang · Liangyuan Jia · Lifang Wu

Received: 11 September 2012 / Accepted: 7 December 2012 / Published online: 23 January 2013

Abstract The purpose of this work is to characterize the interactions of two disulfide-constrained cyclic tetrapeptides [c(Ac-Cys-Pro-Phe-Cys-NH_2), SS1; c(Ac-Cys-Pro-Gly-Cys-NH_2), SS2] with Cu^{2+} ions in order to facilitate the design of cyclic peptides as sensors for metal ions. The Cu^{2+}–peptide complex cations at *m/z* 569.1315 for Cu^{2+}–SS1 and *m/z* 479.0815 for Cu^{2+}–SS2 were detected by mass spectrometry. The gas-phase fragmentation of the Cu^{2+}–peptide complexes was studied by collision-induced dissociation and suggests the atoms involved in the coordination. Cu^{2+} ion binds to a single SS1 or SS2 with $K_{d(app)}$ of 0.57 ± 0.02 and 0.55 ± 0.01 μM, respectively. Isothermal titration calorimetry data indicate both enthalpic and entropic contributions for the binding of Cu^{2+} ion to SS1 and SS2. The characteristic wavenumber of 947 cm^{-1} and the changes at 1,664 and 1,530 cm^{-1} in the infrared spectrum suggest that the sulfydryl of cysteine, the carbonyl group, and amide II are involved in the coordination of Cu^{2+}. The X-ray absorption near-edge structure signal from the Cu^{2+}–peptide complex corresponds to the four-coordination structure. The extended X-ray absorption fine structure and electron paramagnetic resonance results demonstrate the Cu^{2+} ion is in an S/N/2O coordination environment, and is a distinct type II copper center. Theoretical calculations further demonstrate that Cu^{2+} ion binds to SS1 or SS2 in a slightly distorted tetragonal geometry with an S/N/2O environment and the minimum potential energy.

Keywords Cu^{2+} ion · Cyclic peptide · Metal sensor · Mass spectrometry

Introduction

Peptides are effective ligands for metal ions [1]. Cyclic peptides are a specific group of peptides with a cyclic structure for the main peptide chain. Natural cyclic peptides display a broad range of biological roles in living organisms, including as hormones, toxins, antibiotics, and molecules with enzymatic or transport functions [2–7]. Cyclic peptides contain donor atoms in the peptide backbone and the amino acid side chain which are able to complex with metal ions. Metal ion–peptide systems are attractive to researchers with an interest at the interface between inorganic chemistry and biochemistry. Cyclic peptides have potential as metal ion biosensors for the determination of metal ion concentrations in the environment [8, 9].

Among these metal ions, copper is an essential element that is used as a cofactor in many proteins involved in

Electronic supplementary material The online version of this article (doi:10.1007/s00775-012-0972-2) contains supplementary material, which is available to authorized users.

L. Zhang (✉) · L. Wu
Hefei Institutes of Physical Science,
Chinese Academy of Sciences,
Hefei, Anhui 230031,
People's Republic of China
e-mail: zly0605@ustc.edu.cn

L. Zhang · L. Zhang · L. Jia
National Synchrotron Radiation Laboratory,
University of Science and Technology of China,
Hefei, Anhui 230029, People's Republic of China

Z. Luo · L. Wu
School of life Sciences,
University of Science and Technology of China,
Hefei, Anhui 230027,
People's Republic of China

several vital processes [10–13]. Studies on the coordination abilities of cyclic peptides with regard to Cu^{2+} ions have shown that cyclic peptides with a histidyl residue in the peptide sequence are able to bind metal ions via the imidazole nitrogen as well as via the deprotonated amide nitrogens from the main peptide chain [7, 14–16]. Interesting information has been provided by studies on the coordination abilities of cyclic tetrapeptides. The pH and the peptide ring size have a great impact on the kind of coordinated nitrogen [17–19]. Bertram and Pattenden [20] summarized the metal binding and metal complexes of azole-based cyclic peptides of marine origin and pointed out what structural and stereochemical features in marine metabolites are necessary to facilitate metal complexation and transport. The Comba group reported the Cu^{2+} coordination chemistry of the cyclic pseudo-octapeptide patellamide derivatives H_4pat^1 [21], H_4pat^2, and H_4pat^3 [22], drew conclusions on the structure–reactivity correlations, and provided information on why nature might have chosen oxazolines and thiazoles as incorporated heterocycles.

Peptides are versatile and powerful ligands. Donor atoms of independent side chain residues, especially those of imidazole nitrogen of histidine, thiolate sulfur of cysteine, and carboxylate oxygen of aspartate and glutamate, are the major metal binding sites [23]. Cu^{2+} prefers nitrogen donors such as histidine or oxygen donors such as glutamate and aspartate [10]. It is not strange that in oxytocin and vasopressin-like peptides, which are cyclic peptides with a disulfide bridge between cysteine residues, no sulfur atom is involved in the coordination with Cu^{2+} [7, 24]. Sulfur donor ligands such as cysteine and methionine in proteins coordinate with Cu^{+} ion [10, 25, 26]. However, peptides of cysteine generally form very strong covalent bonds with the typically soft-metal ions (e.g., Pd^{2+}, Pt^{2+}, and Hg^{2+}). Cu^{2+} also has relatively high affinity for thiolate residues, especially if mixed (S,N) chelates can be formed [23].

In this work, we present the coordination properties of Cu^{2+} ions and two disulfide-constrained cyclic tetrapeptides (Fig. 1) as determined by high-resolution electrospray ionization mass spectrometry (ESI-MS), isothermal titration calorimetry (ITC), Fourier transform infrared (FTIR) spectroscopy, X-ray absorption fine structure (XAFS) spectroscopy, electron paramagnetic resonance (EPR) spectroscopy, and theoretical calculations. The stoichiometry, affinity, and coordination structure of Cu^{2+}–peptide complexes are discussed in detail.

Materials and methods

Materials

All reagents and solvents were of analytical grade and were used without further purification. Synthesis and purification of cyclic peptides were performed by the same methods as those described by Shi et al. [27]. The purity of the cyclic tetrapeptide was above 99 % (Fig. S1).

Mass spectrometry

All experiments were conducted with a commercial QSTAR Pulsar i hybrid tandem quadrupole time-of-flight mass spectrometer (AB SCIEX, Concord, ON, Canada). The sample was diluted in water/methanol solution (1:1 v/v) to 1–10 μM. The solution was introduced into the source using a direct infusion pump and then sprayed at a flow rate of 1 μL/min. The capillary voltage was maintained between 3.5 and 4.5 kV, and nitrogen gas was used for both desolvation and nebulization.

For the collision-induced dissociation (CID) experiments, the precursor ion of interest was selected using the analyzer and the product ions were analyzed using a time-of-flight analyzer. Nitrogen served as the cooling gas as

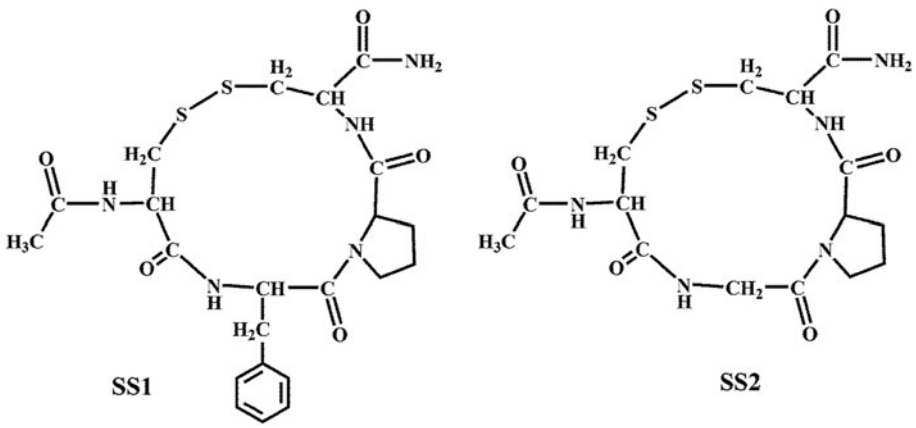

Fig. 1 The structure of the CPxC-motif-based cyclic tetrapeptides SS1 and SS2

well as the collision gas for the CID experiments, and the pressure in the collision cell was maintained at 10 mTorr. The collision energy was 30 eV.

Isothermal titration calorimetry

ITC measurements were performed at 25 ± 0.2 °C using an isothermal titration calorimeter (ITC200 GE). The Cu^{2+} concentrations of stock solutions were verified by titrations against standardized EDTA solutions. Two cyclic tetrapeptides were buffered at pH 7.4 with 20 mM tris(hydroxymethyl)aminomethane–HCl buffer. All solutions were filtered through 0.22-μm filters and degassed prior to use. Typically, 13 portions of 3 μL metal solution were injected into the peptide solution in the sample cell during each titration. A delay of 180 s between injections was allowed for equilibration. The heat generated during interactions was measured by the instrument. The titration of metal ions into buffer was done in each experiment as a reference for baseline corrections in the data processing. All experiments were repeated at least three times.

The ITC data were analyzed using the Origin 7.0 software package from MicroCal. Baseline correction was applied for each experiment by subtraction of data from the titration of metal ion solution into a buffer blank correlating to the heat of dilution. A binding isotherm was fitted to the data using a nonlinear least-squares method to minimize χ^2 values. The detected enthalpy change (ΔH_{ITC}) and association constant (K_{ITC}) were obtained from the best-fit parameters. The Cu^{2+} binding constant with regard to cyclic peptide was calculated as $K_a = K_{ITC} \times K_{buffer}$ and the dissociation constant was calculated as $K_d = 1/K_{bind}$ as described previously [28].

Fourier transform infrared spectroscopy

FTIR measurements were performed at room temperature with a PerkinElmer Spectrum instrument equipped with an HgCdTe (nitrogen-cooled) detector and a KBr beam splitter. The spectra were recorded with a resolution of 2 cm^{-1}. Two hundred and fifty-six scans on an air-dried film (wet film) were co-added, with use of AgBr windows under green light. The treatment and analyses of the FTIR spectra were described in previous studies [29, 30].

X-ray absorption fine structure spectroscopy

The copper K-edge XAFS spectra were measured at beamline U7C of the National Synchrotron Radiation Laboratory of China. The electron beam energy was 0.8 GeV and the maximum stored current was 250 mA. The incident X-ray beam was generated by a nondispersive silicon double-crystal monochromator with 111 symmetric reflections. The X-ray harmonics were minimized by detuning the two flat Si(111) crystal monochromators to about 70 % of the maximum incident light intensity. The XAFS spectra were measured at room temperature in fluorescence mode by using a seven-element pixel high-purity germanium solid-state detector with 45° incidence angle. Cu^{2+}–peptide complexes were lyophilized shortly after adding Cu^{2+} ions to peptide solution (1:1 Cu^{2+} to peptide) and were measured in powder samples. The X-ray energy for the copper K edge was internally calibrated to 8,979 eV by using transmission data from a copper foil. The data shown are the average of three to five scans and were analyzed using a previously described method [31].

Electron paramagnetic resonance spectroscopy

EPR spectra were recorded with a Bruker EMXplus 10/12 EPR spectrometer equipped with an Oxford Instruments EPR901 liquid helium continuous-flow cryostat fitted with a super-high-*Q* cavity. The magnetic field was measured by a Hall probe calibrated with the 1,3-bisdiphenylene-2-phenylallyl EPR signal and a Bruker ER 036TM teslameter. The microwave frequency was measured with an internal frequency counter. The temperature was controlled with an Oxford Instruments ITC503S temperature controller. The spectra were acquired with a sweep width of 2,000 G, a frequency of 9.383303 GHz, a modulation amplitude of 5 G, a modulation frequency of 100 kHz, and a temperature of 40 K. The EPR spectra of Cu^{2+}–peptide complexes were simulated using biomolecular EPR spectroscopy software (Hyperfine Spectrum program).

Theoretical calculations

The copper(II) complexes were calculated with the hybrid density functional B3LYP method with the 6–31G(d,p) basis set for carbon, nitrogen, oxygen, sulfur, and hydrogen [32]. The double-ζ valence basis sets and the effective core potentials of Hay and Wadt [33] (Lanl2DZ) were used for the copper atom. The *f* polarization function was also added to increase the flexibility of the effective core potential basis. The *f* exponent is 3.525 for the copper atom [34]. All calculations were performed with the program Gaussian 03 [35].

Results

Mass spectrometry

High-resolution electrospray ionization time-of-flight mass spectrometry was used to identify charged complexes. Figure 2 shows the mass spectra of protonated cyclic

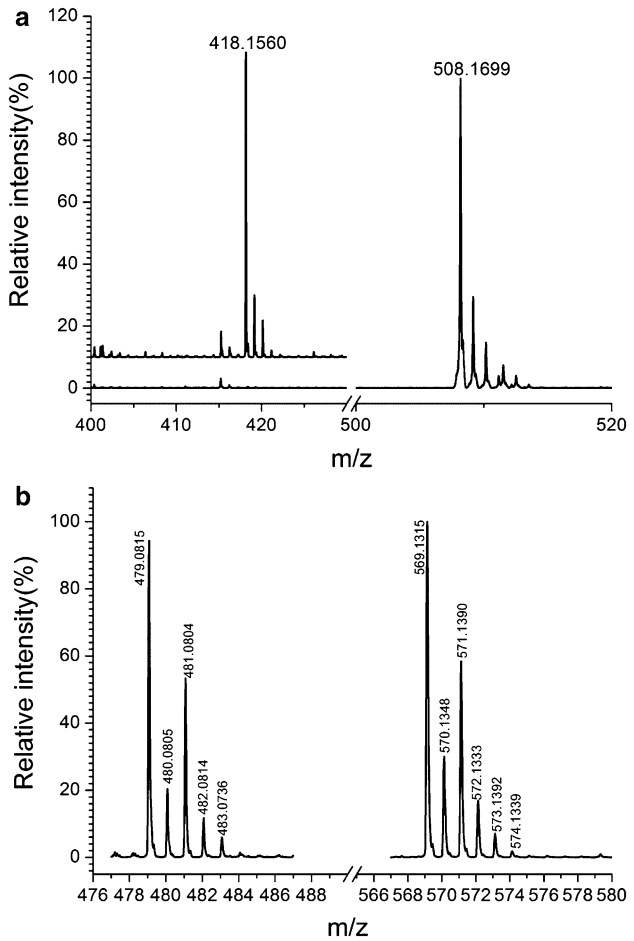

Fig. 2 The mass spectra of cyclic peptides (**a**) and Cu^{2+}–peptide complexes (**b**)

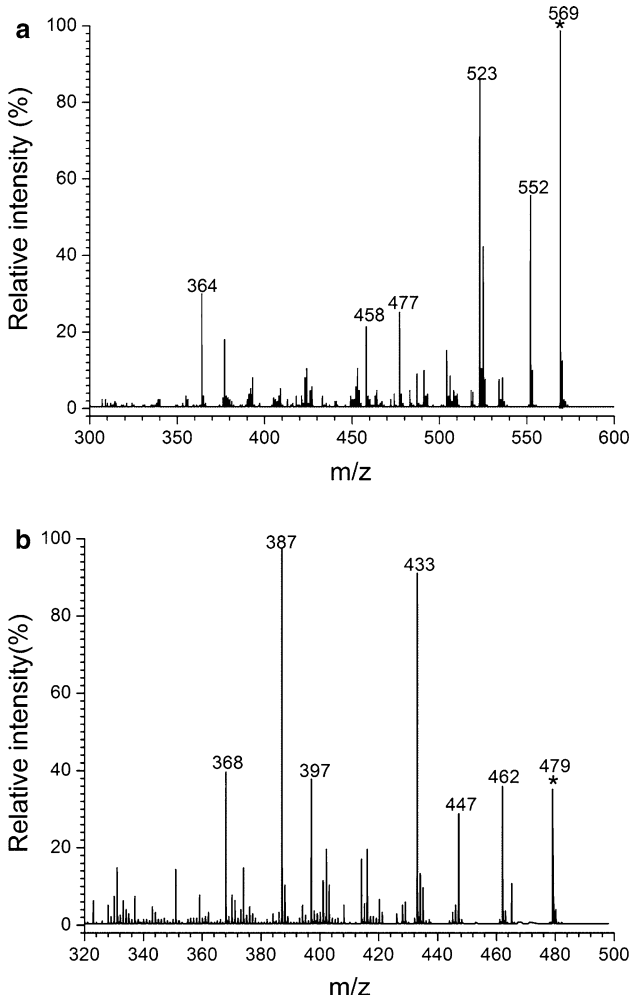

Fig. 3 Collision-induced-dissociation spectra of the Cu^{2+}–peptide complexes: (**a**) Cu^{2+}–SS1 complex and (**b**) Cu^{2+}–SS2 complex. The *asterisk* designates the parent ion

tetrapeptides and Cu^{2+}–peptide complexes. The peaks at *m/z* 508.1699 and 418.1560 respond to $[SS1+H]^+$ and $[SS2+H]^+$, respectively. However, the peaks at *m/z* 569.1315 and 479.0815 prove the existence of $[Cu^{2+}(SS1-H)]^+$ and $[Cu^{2+}(SS2-H)]^+$ in the solution of Cu^{2+} ions and the cyclic tetrapeptides. These results indicate that deprotonation is followed by Cu^{2+} coordinating with the cyclic tetrapeptides, and that these protons may be captured by the metal-free cyclic tetrapeptides. Precise masses and isotope distributions for the Cu^{2+}–peptide complexes are listed in Table S1. The results also indicate that the binding stoichiometry of Cu^{2+} ion with regard to cyclic tetrapeptide is 1:1.

The CID of the parent ions of the Cu^{2+}–peptide complexes was done to understand the gas-phase molecular reactivity of Cu^{2+}–peptide complexes, as shown in Fig. 3. The main fragment ions containing copper ion were at *m/z* 552, 523, 477, 458, and 364 for the Cu^{2+}–SS1 complex (Fig. 3a) and at *m/z* 462, 447, 433, 397, 387, and 368 for the Cu^{2+}–SS2 complex (Fig. 3b). The assignments of the fragment ions are listed in Table 1. These results demonstrated the two Cu^{2+}–peptide complexes shared the same fragmentation pathway of losing the hydroxyl radical, the CH_2SSCH_2 group, and the $CH_3CONHCCHCO$ radical. However, the fragmentation pathway of losing the sulfur atom or the SCH_2 radical from the $[Cu^{2+}(SS1-H)]^+$ parent ion was not observed. Maybe the delocalized electron of the phenyl group affected the gas-phase dissociation of the $[Cu^{2+}(SS1-H)]^+$ parent ion.

Isothermal titration calorimetry

ITC is an efficient technique for the determination of the stoichiometry and thermodynamic parameters of ligand binding to biomolecules [28, 36]. The representative ITC data in Fig. 4 demonstrate the isotherms of Cu^{2+} ion binding to SS1 and SS2. The least-squares fitting of the titration data resulted in a single-site binding model, and the stoichiometry was 1:1 for Cu^{2+} and cyclic peptide. The

overall dissociation constants (K_d) were calculated from the association constants derived from the ITC results. $K_a = K_{ITC} \times K_{buffer}$, $K_d = 1/K_a$. Log K_{buffer} for addition of Cu^{2+} to tris(hydroxymethyl)aminomethane buffer at pH 7.4 was 1.8 [37]. The association constants of Cu^{2+} and the two peptide were calculated to be $1.74 \pm 0.02 \times 10^6$ and $1.81 \pm 0.03 \times 10^6$ M^{-1}, corresponding to dissociation constants (K_d) of 0.57 ± 0.02 and 0.55 ± 0.01 μM for SS1 and SS2, respectively. The values of the enthalpy change (ΔH) and the entropy change (ΔS) indicated both enthalpic and entropic contributions for Cu^{2+} ions binding to SS1 and SS2 (Table S2).

Table 1 The assignments of fragment ions for the collision-induced dissociation of the parent ions of the Cu^{2+}–peptide complexes

Complexes	*m/z*	Ion assignment
Cu^{2+}–SS1	552	$[Cu^{II}(SS1-H)-OH]^{+\bullet}$
	523	$[Cu^{II}(SS1-H)-HCONH_3]^{+}$
	477	$[Cu^{II}(SS1-H)-CH_2SSCH_2]^{+}$
	458	$[Cu^{II}(SS1-H)-CH_3CONHCCHCO]^{+\bullet}$
	364	$[Cu^{II}(SS1-H)-CH_3CONHCH(CONH)CH_2SSCH]^{+\bullet}$
Cu^{2+}–SS2	462	$[Cu^{II}(SS2-H)-OH]^{+\bullet}$
	447	$[Cu^{II}(SS2-H)-S]^{+}$
	433	$[Cu^{II}(SS2-H)-SCH_2]^{+}$
	397	$[Cu^{II}(SS2-H)-CH_3CONCCH]^{+\bullet}$
	387	$[Cu^{II}(SS2-H)-CH_2SSCH_2]^{+}$
	368	$[Cu^{II}(SS1-H)-CH_3CONHCCHCO]^{+\bullet}$

For the structures of SS1 and SS2, see Fig. 1.

Fourier transform infrared spectroscopy

The FTIR spectra of the free SS1 and its metal complex are shown in Fig. 5a. The broad band with medium intensity at 3,292 cm^{-1} was assigned to amide A (N–H stretching vibration). Amide I (mainly C–O stretching vibration) is observed as a strong band at 1,664 cm^{-1}, whereas amide II (N–H bending and C–N stretching modes) appears at 1,531 cm^{-1}. Evidence for Cu^{2+} binding to SS1 comes from the weak positive derivative feature at 947 cm^{-1} and the shifts of the features at 1,172–1,230 and 1,433–1,440 cm^{-1} in the infrared spectrum of the Cu^{2+}–SS1 complexes. In the 600–1,000 cm^{-1} region, protein C–S–H bending and C–S stretching are observed [30]. Therefore, the weak positive derivative feature at 947 cm^{-1} corresponds to the coordination of Cu^{2+} to the sulfur atom. However, the main differences for the Cu^{2+}–SS2 complex are the changes at 1,530 and 1,664 cm^{-1} due to the coordination of Cu^{2+} to the nitrogen atom of amide II and the oxygen atom of the carbonyl group (Fig. 5b). A previous study reported that ring size impacted on the copper(II) coordination abilities of cyclic tetrapeptides [17]. For the peptides with more than 13-membered rings, the formation of a complex with the 4N binding mode is preferred [38]. A 14-membered, tetraza cyclic tetrapeptide as a dominant species was formed around physiological pH with Cu^{2+} ions coordinated to two amide nitrogens, an imidazole nitrogen, and a water molecule [17]. In this work, SS1 and SS2, with a 14-membered ring, were likely to offer the sulfur, nitrogen, and oxygen atoms from the ring to coordinate with Cu^{2+} at pH 7.4.

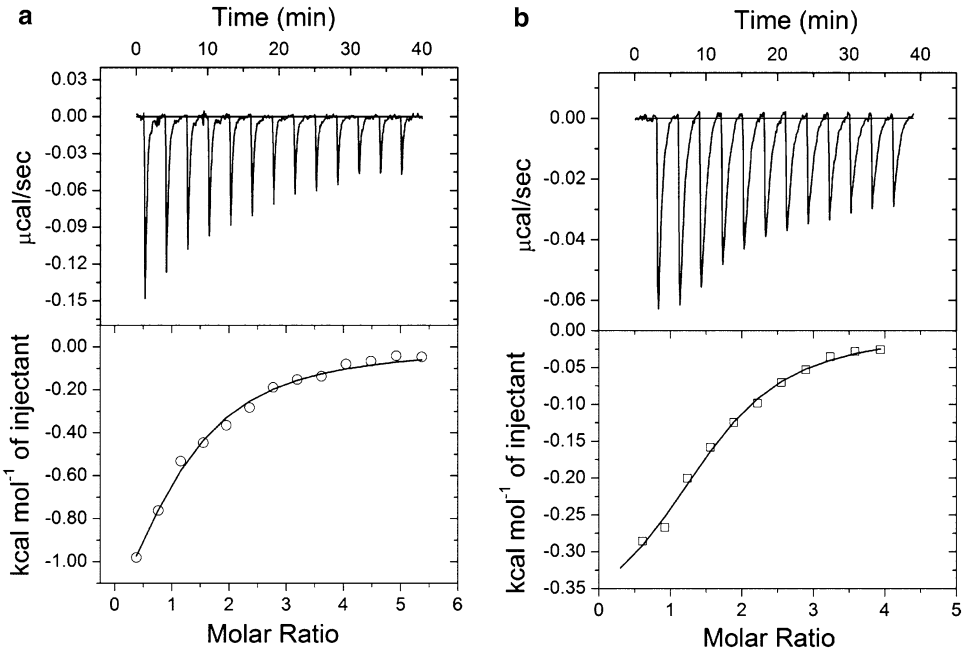

Fig. 4 Isothermal titration calorimetry (ITC) measurement of Cu^{2+} binding to SS1 (**a**) and SS2 (**b**). *Upper panels*: Raw ITC data for injection of 1.25 mM Cu^{2+} ions into 50 μM SS1 or 40 μM SS2 at 25 °C. *Lower panels*: Normalized ITC data for titrations versus molar ratio of Cu^{2+}–SS1 or Cu^{2+}–SS2. Data analysis using Origin 7.0 indicates that the binding data fit well to a single-site binding model

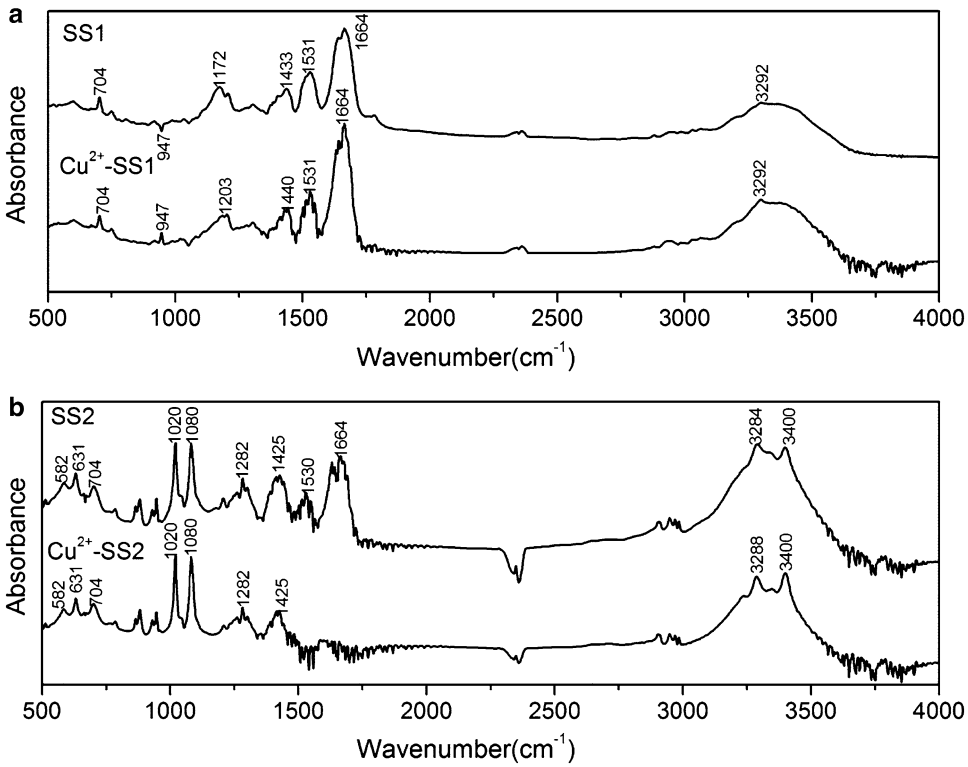

Fig. 5 Fourier transform infrared spectra (KBr pellets) of **a** SS1 and the Cu(II)–SS1 complex and **b** SS2 and the Cu(II)–SS2 complex in the 500–4,000 cm^{-1} region

X-ray absorption fine structure spectroscopy

The XAFS spectroscopy approach is extremely sensitive to the geometric environment of the absorbing atom. The K-edge X-ray absorption near-edge structure (XANES) spectra of the Cu^{2+}-SS1 and Cu^{2+}–SS2 complexes are shown in (Fig. 6, inset). The Cu^{2+}–peptide complexes show the pre-edge at 8,980 eV and the first intense transition occurs at 8,986 eV, which are typical of absorptions of Cu^{2+} complexes [31]. This observation confirms the divalent state of the copper ion in the Cu^{2+}–peptide complex under the experimental conditions. The XANES signal from the Cu^{2+}–peptide complex corresponds to the four-coordination structure of copper(II) complexes [39, 40].

Extended XAFS (EXAFS) analysis is used to provide information about the metal sites regarding the types of atoms in the primary coordination sphere, bond lengths, and the presence of ligands in the primary coordination sphere (from multiple scattering analysis) [41]. As shown in Fig. 6, the data were well fit with a four-coordinate site, containing an S/N/2O coordination environment. The theoretical simulation was obtained from inverse Fourier transforms based on the model of first- and second-nearest coordination shells, and the best fits were superimposed on the data. The other parameters obtained from the fitting are listed in Table 2. The fitting of the spectrum revealed that

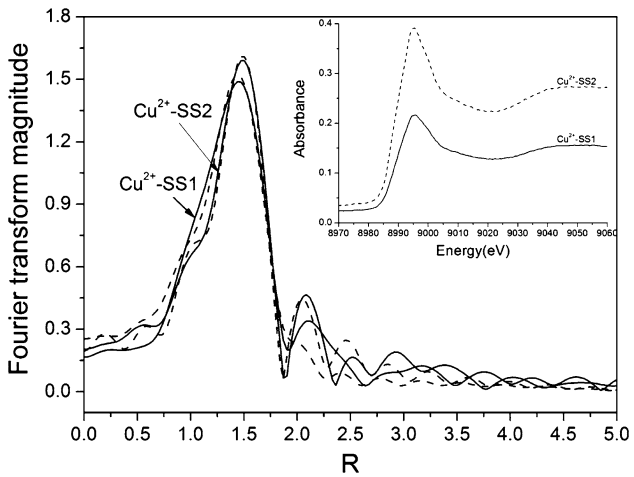

Fig. 6 The Fourier transform of the extended X-ray absorption fine structure oscillation function $k^3\chi(k)$. *Solid line* experimental data, *dashed line* simulation result. The *inset* shows the copper K-edge X-ray absorption near-edge structure data from the Cu^{2+}–SS1 complex (*solid line*) and the Cu^{2+}–SS2 complex (*dashed line*)

the Cu^{2+} ion was bound to four atoms, including one nitrogen atom at 1.98 (2) Å, two oxygen atoms at 2.01 (2) Å, and one sulfur atom at 2.49 (3) Å. These results were consistent with the FTIR results, in which the Cu^{2+}–S interaction showed the characteristic wavenumber of 947 cm^{-1}.

Table 2 The fine fitting results of the extended X-ray absorption fine structure spectra of the Cu^{2+}–SS1 and Cu^{2+}–SS1 complexes obtained by using the FEFF 8 software package

Complex	Coordination number	Ligand	Debye–Waller factor σ^2 (Å^2)	Bond length (Å)
Cu^{2+}–SS1	4	2O	0.0012 (3)	2.01 (2)
		1N	0.0036 (1)	1.99 (3)
		1S	0.0015 (4)	2.46 (1)
Cu^{2+}–SS2	4	2O	0.0042 (3)	2.01 (2)
		1N	0.0029 (3)	1.98 (2)
		1S	0.0015 (2)	2.49 (3)

Electron paramagnetic resonance spectroscopy

X-band EPR spectroscopy was used to support the interpretation based on ESI-MS, FTIR spectroscopy, and XAFS spectroscopy. EPR spectra were obtained at pH 7.4 and 40 K for both Cu^{2+} complexes with the peptides SS1 and SS2 and showed a distinct type II copper center (Fig. 7). Simulation of the spectra indicated that the sites were axial with $g_\perp = 2.062$ ($A_\perp = 10 \times 10^{-4}$ cm^{-1}) and $g_\parallel = 2.322$ ($A_\parallel = 147 \times 10^{-4}$ cm^{-1}) for the Cu^{2+}–SS1 complex and $g_\perp = 2.060$ ($A_\perp = 10 \times 10^{-4}$ cm^{-1}) and $g_\parallel = 2.322$ ($A_\parallel = 145 \times 10^{-4}$ cm^{-1}) for the Cu^{2+}–SS2 complex. In accordance with analysis of Cu^{2+} EPR spectra by Peisach and Blumberg [42], the range of $g_\parallel$ and $A_\parallel$ indicated a Cu^{2+} ion with S/N/2O coordination in Cu^{2+}–SS1 and Cu^{2+}–SS2 [43]. $g_\parallel > g_\perp > g_e$ ($g_e = 2.0023$) indicated that Cu^{2+}–SS1 and Cu^{2+}–SS2 have a tetragonal Cu(II) environment [44].

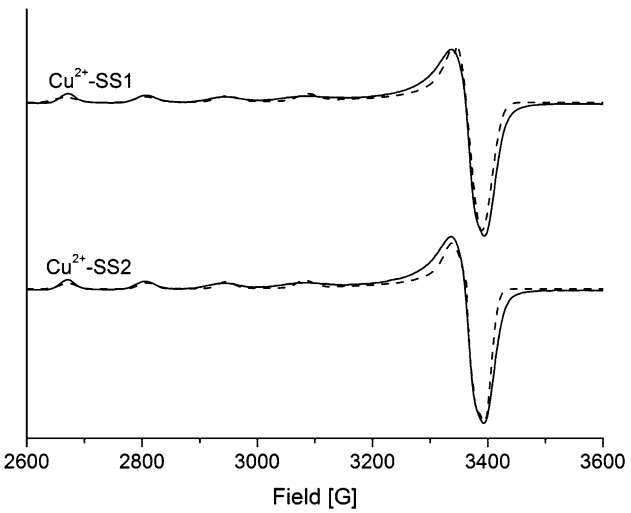

Fig. 7 Electron paramagnetic resonance spectrum (*solid line*) with simulation (*dashed line*) of 100 μM Cu^{2+}–SS1 and Cu^{2+}–SS2 complexes in 30 % glycerol/H_2O solution (pH 7.4). Microwave frequency 9.383303 GHz, microwave power 1 mW, modulation frequency 100 kHz, modulation amplitude 5 G, temperature 40 K

Theoretical calculations

The type II copper sites are typified by tetragonal coordination of Cu^{2+} with four ligands that are either coplanar or slightly distorted from a coplanar array. We therefore performed density functional theory calculations for the optimized structure and conformation of peptides and their complexes to gain insight into the energetics of the conformational change of the cyclic peptides upon coordination to Cu^{2+} ion. The best proposed SS1, SS2, Cu^{2+}–SS1, and Cu^{2+}–SS2 structures obtained from the theoretical calculations are shown in Fig. 8 and other computed structures are shown in Fig. S2. The calculated relative energies are listed in Table S3. Density functional theory calculations were performed with a setup previously optimized for copper(II) complexes [45, 46]. Frequency calculations on the optimized structures were used to verify that they were indeed minima on the potential energy surface. For the best proposed structure, every angle and length of the coordinate bonds is listed in Table S4. According to the data, the Cu^{2+}–SS1 and Cu^{2+}–SS2 complexes had a four-coordination slightly distorted tetragonal geometry, with one sulfur and one nitrogen atom as well as two oxygen donors, and it was in agreement with the simulation and interpretation of the EPR and EXAFS data.

Discussion

Simple metal–peptide systems provide a basis for understanding metal interactions occurring in biochemically relevant systems. We are especially interested in developing cyclic-peptide-based motifs for selective metal ion binding and sensing. SS1 and SS2 are cyclic disulfide peptides. In principle, they are expected to bind heavy metals such as Hg^{2+}, Pb^{2+}, Cu^{2+}, and Cd^{2+}. In fact, the amino acid sequence CxxC is conserved in many soft-metal transporters that are involved in the control of the intracellular concentration of ions such as Cu^{+}, Hg^{2+}, Zn^{2+}, and Pb^{2+} [47].

The Cu^{2+}–SS1 and Cu^{2+}–SS2 complexes were detected by ESI-MS. Their accurate *m/z* values indicated Cu^{2+} ions were ligated by deprotonated SS1 or SS2 and formed a singly charged Cu^{2+}–peptide complex $[Cu^{2+}(M-H)]^+$. These results also indicated that Cu^{2+}–peptide complexes detected in the mass spectrometer were formed in solution and that the state of cyclic peptide protonation in these complexes does not change during the electrospray process. Gas-phase copper complexes have been shown to exhibit interesting properties regarding their formation, structure, and dissociation in the absence of any interference from solvents or other species present in solution. In

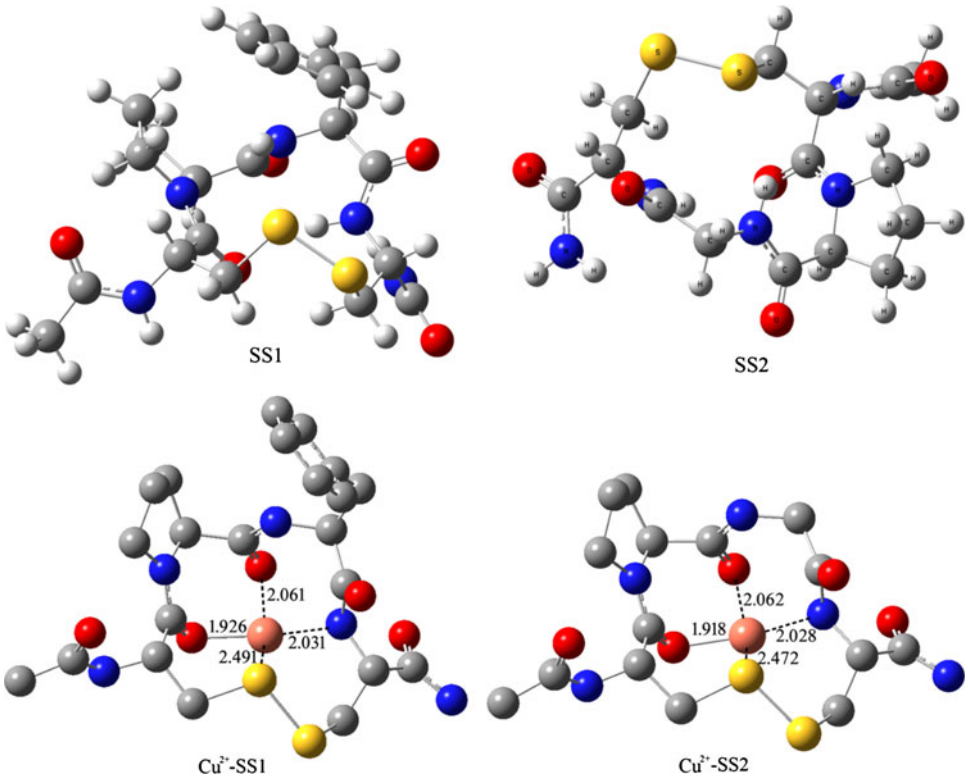

Fig. 8 The calculated structures of SS1, SS2, and the Cu^{2+}–peptide complexes. In the structure of the complexes, all hydrogen atoms have been removed for clarity. The Cu^{2+} ion is shown in *pink*. Oxygen, carbon, and nitrogen atoms are shown in *red*, *gray*, and *blue*, respectively

particular, electrospray ionization had been found to produce copper complexes [7, 48, 49]. We mass-selected the $[Cu^{2+}(M-H)]^{+}$ species seen in Fig. 2 and subsequently performed a CID experiment and obtained the fragmentation spectrum displayed in Fig. 3. The fragmentation pathway suggested sulfur, nitrogen, and oxygen atoms are involved in the binding since the two Cu^{2}–peptide complexes lose the same fragments: hydroxyl radical, CH_2SSCH_2 group, and $CH_3CONHCCHCO$ radical.

The ESI-MS and ITC data indicated that the stoichiometry for Cu^{2+} binding to cyclic tetrapeptides was 1:1. This agreed with that of Cu^{2+} binding to histidyl-containing cyclic peptides [14, 16, 17, 19]. ITC reported Cu^{2+} binding affinities of $K_d \sim 10^{-7}$ M for SS1 and SS2. The affinity is at a level similar to that for MxCxxC-based cyclic peptide binding to Zn^{2+}, but is weaker than that for Hg^{2+}, Pb^{2+}, Cu^{+}, and Cd^{2+} [47].

The pH and the peptide ring size had a great impact on the kind of coordination [17–19]. In this work, SS1 and SS2 had a 14-membered ring backbone and the Cu^{2+} ions interacted with SS1 and SS2 at pH 7.4 such that we could estimate the coordination environment using different methods under the same conditions. The fitting of the EXAFS data revealed that the Cu^{2+} ion was bound to four atoms, including one nitrogen atom at 1.98 (2) Å, two oxygen atoms at 2.01 (2) Å, and one sulfur atom at 2.49 (3) Å. This was consistent with the FTIR result, in which the positive derivative feature at 947 cm^{-1} indicated the Cu^{2+}–S interaction. Cu^{2+}–S interaction also occurred and gave a characteristic absorption peak at 356 nm due to S → Cu^{2+} charge transfer in the copper-intein system [31]. However, in the UV–vis spectrum of Cu^{2+}–SS1 and Cu^{2+}–SS2, there are no characteristic absorption peaks for S → Cu^{2+} charge transfer in the 350–450-nm range (data not shown). The XANES signal from the Cu^{2+}–peptide complex corresponds to the four-coordination structure of Cu^{2+} complexes. EPR spectroscopy was used to further demonstrate the coordination environment and the simulation of EPR spectra indicated that the Cu^{2+}–peptide complex contained a distinct type II copper center. The Sóvágó group has performed systematic studies on copper(II) complexes of Gly_nHis peptides and found the EPR spectral parameter $g_{\|}$ decreased (from 2.299 to 2.199), indicating the structure of the complexes changed from 2N to 4N coordination [23]. $g_{\|}$ for Cu^{2+}–SS1 and Cu^{2+}–SS2 is 2.322, bigger than 2.299. This indicates that in Cu^{2+}–SS1 and Cu^{2+}–SS2 only one nitrogen atom may be involved in coordination. Furthermore, the theoretical calculations estimated the optimal structure to be a slightly distorted tetragonal structure and affirmed the coordination sphere arrangement by frequency calculations and minimum-energy optimization. Recently, a few studies of noncovalent interactions of metal atoms binding to the phenyl ring by cation–π interactions were reported [50–52]. In Fig. 8, the distance between the Cu^{2+} ion and the aromatic carbon atom is 6.40 Å, which is greater than the sum of the van der

Waals radii (4.05 Å). No cation–π interaction existed in Cu^{2+}–SS1. Therefore, it can be well understood why Cu^{2+}–SS1 and Cu^{2+}–SS2 have the same coordination model although they have different structures.

In conclusion, we studied the binding properties of Cu^{2+} with regard to two disulfide-constrained cyclic tetrapeptides. The Cu^{2+}–SS1 and Cu^{2+}–SS2 complexes were identified by ESI-MS and the gas-phase chemical properties were analyzed by CID. The binding stoichiometry, affinity, and thermodynamic parameters were obtained by ITC. The experiments (FTIR spectroscopy, XAFS spectroscopy, and EPR spectroscopy) and theoretical calculations demonstrated Cu^{2+} ions binding to disulfide-constrained cyclic tetrapeptides in a slightly distorted tetragonal geometry with an S/N/2O environment. These results provide useful information to develop a cyclic-peptide-based new metal ion biosensor for the determination of metal ion concentrations in the environment.

Acknowledgments This study was supported by the Natural Science Foundation of China (nos. 11105150 and 21004056), the China Postdoctoral Science Foundation (no. 2012M510163), and the Fundamental Research Funds for the Central Universities (no. WK2310000012). We thank the Chinese Academy of Sciences for the One Hundred Talent Project (no. KJCX2-YW-N47). We thank Wei Tong in the High Magnetic Field Laboratory, Chinese Academy of Sciences, for the EPR measurements. We are grateful to Fei Qi, Xiaolong Xu and Zhengyan Wu for continuous support and helpful discussions.

References

1. Kozlowski H, Kowalik-Jankowska T, Jezowska-Bojczuk M (2005) Coord Chem Rev 249:2323–2334
2. Liehr S, Barbosa J, Smith AB, Cooperman BS (1999) Org Lett 1:1201–1204
3. Tamilarasu N, Huq I, Rana TM (2000) Bioorg Med Chem Lett 10:971–974
4. Jelokhani-Niaraki M, Kondejewski LH, Wheaton LC, Hodges RS (2009) J Med Chem 52:2090–2097
5. Hashizume H, Adachi H, Igarashi M, Nishimura Y, Akamatsu Y (2010) J Antibiot 63:279–283
6. Ovchinnikov YA, Ivanov VT (1975) Tetrahedron 31:2177–2209
7. Wyttenbach T, Liu D, Bowers MT (2008) J Am Chem Soc 130:5993–6000
8. Viguier B, Zor K, Kasotakis E, Mitraki A, Clausen CH, Svendsen WE, Castillo-Leon J (2011) ACS Appl Mater Interfaces 3:1594–1600
9. Ngu-Schwemlein Maria, Gilbert Willie, Askew K, Schwemlein S (2008) Bioorg Med Chem Lett 16:5778–5787
10. Kim BE, Nevitt T, Thiele DJ (2008) Nat Chem Biol 4:176–185
11. Yatsunyk LA, Rosenzweig AC (2007) J Biol Chem 282:8622–8631
12. Pappalardo G, Impellizzeri G, Campagna T (2004) Inorg Chim Acta 357:185–194
13. Sarkar B (1999) Chem Rev 99:2535–2544
14. Brasun J, Matera-Witkiewicz A, Kamysz E, Kamysz W, Oldziej S (2010) Polyhedron 29:1535–1542
15. Afonso C, Tabet JC, Giorgi G, Turecek F (2012) J Mass Spectrom 47:208–220
16. Brasun J, Matera A, Oldziej S, Swiatek-Kozlowska J, Messori L, Gabbiani C, Orfei M, Ginanneschi M (2007) J Inorg Biochem 101:452–460
17. Brasuń J, Matera-Witkiewicz A, Ołdziej S, Pratesi A, Ginanneschi M, Messori L (2009) J Inorg Biochem 103:813–817
18. Bonomo RP, Impellizzeri G, Pappalardo G, Purrello R, Rizzarelli E, Tabbi G (1998) Dalton Trans 3851–3857
19. Pratesi A, Zanello P, Giorgi G, Messori L, Laschi F, Casini A, Corsini M, Gabbiani C, Orfei M, Rosani C, Ginanneschi M (2007) Inorg Chem 46:10038–10040
20. Bertram A, Pattenden G (2007) Nat Prod Rep 24:18–30
21. Comba P, Dovalil N, Hanson GR, Linti G (2011) Inorg Chem 50:5165–5174
22. Comba P, Dovalil N, Gahan LR, Haberhauer G, Hanson GR, Noble CJ, Seibold B, Vadivelu P (2012) Chem Eur J 18:2578–2590
23. Sovago I, Kallay C, Varnagy K (2012) Coord Chem Rev 256:2225–2233
24. Kozlowski H, Radomska B, Kupryszewski G, Lammek B, Livera C, Pettit LD, Pyburn S (1989) Dalton Trans 173–177
25. Finney LA, O'Halloran TV (2003) Science 300:931–936
26. Badarau A, Dennison C (2011) J Am Chem Soc 133:2983–2988
27. Shi TS, Spain SM, Rabenstein DL (2004) J Am Chem Soc 126:790–796
28. Zhang LY, Zheng YC, Xi ZY, Luo ZF, Xu XL, Wang CY, Liu YZ (2009) Mol Biosyst 5:644–650
29. Nahar S, Tajmirriahi HA (1995) J Inorg Biochem 58:223–234
30. Nahar S, TajmirRiahi HA (1996) J Colloid Interface Sci 178:648–656
31. Zhang LY, Xiao N, Pan Y, Zheng YC, Pan ZY, Luo ZF, Xu XL, Liu YZ (2010) Chem Eur J 16:4297–4306
32. Becke AD (1993) J Chem Phys 98:5648–5652
33. Hay PJ, Wadt WR (1985) J Chem Phys 82:299–310
34. Ehlers AW, Böhme M, Dapprich S, Gobbi A, Höllwarth A, Jonas V, Köhler KF, Stegmann R, Veldkamp A, Frenking G (1993) Chem Phys Lett 208:111–114
35. Frisch MJ, Trucks GW, Schlegel HB et al (2004) Gaussian 03. Gaussian, Wallingford
36. Leavitt S, Freire E (2001) Curr Opin Struct Biol 11:560–566
37. Thompsett AR, Abdelraheim SR, Daniels M, Brown DR (2005) J Biol Chem 280:42750–42758
38. Schapp J, Haas K, Sünkel K, Beck W (2003) Eur J Inorg Chem 2003:3745–3751
39. Borghi E, Casella L (2010) Phys Chem Chem Phys 12:1525–1534
40. Al-Ebraheem A, Goettlicher J, Geraki K, Ralph S, Farquharson MJ (2010) X-Ray Spectrom 39:332–337
41. Herbst RW, Perovic I, Martin-Diaconescu V, O'Brien K, Chivers PT, Pochapsky SS, Pochapsky TC, Maroney MJ (2010) J Am Chem Soc 132:10338–10351
42. Peisach J, Blumberg WE (1974) Arch Biochem Biophys 165:691–708
43. Bennett B, Hill BC (2011) FEBS Lett 585:861–864
44. Garribba E, Micera G (2006) J Chem Educ 83:1229–1232
45. Comba P, Gahan LR, Haberhauer G, Hanson GR, Noble CJ, Seibold B, van den Brenk AL (2008) Chem Eur J 14:4393–4403
46. Atanasov M, Comba P, Martin B, Müller V, Rajaraman G, Rohwer H, Wunderlich S (2006) J Comput Chem 27:1263–1277
47. Rousselot-Pailley P, Seneque O, Lebrun C, Crouzy S, Boturyn D, Dumy P, Ferrand M, Delangle P (2006) Inorg Chem 45:5510–5520
48. Vaisar T, Gatlin CL, Rao RD, Seymour JL, Tureček F (2001) J Mass Spectrom 36:306–316

49. Banerjee R, Sudarslal S, Ranganayaki RS, Raghothama S (2011) Org Biomol Chem 9:6234–6245
50. Tomic ZD, Novakovic SB, Zaric SD (2004) Eur J Inorg Chem 11:2215–2218
51. Lovell T, Himo F, Han W-G, Noodleman L (2003) Coord Chem Rev 238–239:211–232
52. Ma JC, Dougherty DA (1997) Chem Rev 97:1303–1324